Article:
Kolo, I. and de Borst, R. (2018) An isogeometric analysis approach to gradient-dependent plasticity. International Journal for Numerical Methods in Engineering, 113 (2). pp. 296-310. ISSN: 0029-5981

https://doi.org/10.1002/nme.5614

INTERNATIONAL JOURNAL FOR NUMERICAL METHODS IN ENGINEERING
Int. J. Numer. Meth. Engng 2017; **00**:1–18
Published online in Wiley InterScience (www.interscience.wiley.com). DOI: 10.1002/nme

An isogeometric analysis approach to gradient-dependent plasticity

Isa Kolo and René de Borst*

Department of Civil and Structural Engineering, University of Sheffield, Sheffield S1 3JD, UK

SUMMARY

Gradient-dependent plasticity can be used to achieve mesh-objective results upon loss of well-posedness of the initial/boundary value problem due to the introduction of strain softening, non-associated flow and geometric non-linearity. A prominent class of gradient plasticity models considers a dependence of the yield strength on the Laplacian of the hardening parameter, usually an invariant of the plastic strain tensor. This inclusion causes the consistency condition to become a partial differential equation, in addition to the momentum balance. At the internal moving boundary one has to impose appropriate boundary conditions on the hardening parameter, or equivalently, on the plastic multiplier. This internal boundary condition can be enforced without tracking the elastic-plastic boundary by requiring C^1-continuity with respect to the plastic multiplier. In this contribution this continuity has been achieved by using NURBS as shape functions both for the plastic multiplier and for the displacements. One advantage of this isogeometric analysis approach is that the displacements can be interpolated one order higher, making it consistent with the interpolation of the plastic multiplier. This is different from previous approaches which have been exploited. The regularising effect of gradient plasticity is shown for one and two-dimensional boundary value problems. Copyright © 2017 John Wiley & Sons, Ltd.

Received . . .

KEY WORDS: Gradient plasticity; higher-order continuum; mesh objectivity; isogeometric analysis; Bézier extraction; NURBS

1. INTRODUCTION

In the numerical analysis of strain-softening solids, the use of conventional rate-independent constitutive models can lead to mesh-dependent results. This is because strain softening triggers the development of localised zones, and the absence of an internal length scale in conventional strain-softening models makes these localisation bands to have a zero width. As a consequence, the width of the localised zone that results from simulations equals the smallest width allowed by the discretisation. The origin of the problem lies in the governing boundary value problem which becomes ill-posed at the onset of strain softening, or in some cases when stress-strain relations with a non-symmetric tangential operator are employed, possibly in combination with a large-strain description. In quasi-static problems the character of the partial differential equations then locally changes from elliptic into hyperbolic, giving rise to the possibility of displacement discontinuities [1, 2, 3, 4].

Among other approaches, higher-order continuum theories, which incorporate a material length scale, can maintain well-posedness, even when a localisation zone develops. Thus, they can offer a regularisation of the governing field equations. Gradient plasticity models form one class of such

*Correspondence to: René de Borst, Department of Civil and Structural Engineering, University of Sheffield, Sheffield S1 3JD, UK. E-mail: r.deborst@sheffield.ac.uk

theories. Herein, we focus on a gradient plasticity model in which the yield function depends on second-order spatial derivatives of the hardening parameter, in particular on its Laplacian. As a result, the consistency condition becomes a partial differential equation [5].

In numerical implementations of this gradient-enhanced plasticity theory, the hardening parameter, which is an invariant measure of the plastic strain, is considered as a fundamental unknown and hence becomes an independent degree of freedom that is discretised in addition to the displacements. Different from standard plasticity models, both the equilibrium equation and the consistency condition are now cast in a weak format, and are solved simultaneously. The second-order derivatives of the hardening parameter which appear in the consistency parameter can, in principle, be reduced by an order through a standard application of Gauss' theorem. However, there is an issue at the internal boundary in the body between the elastic and the plastified parts, where a boundary condition on the hardening parameter has to be enforced. As in [2, 4] this internal boundary condition is not enforced explicitly, but is met by interpolating the hardening parameter by $\mathcal{C}^1$-continuous shape functions on the entire domain.

Interpolating the hardening parameter with $\mathcal{C}^1$-continuous shape functions is not straightforward using conventional finite elements. Only a limited class of elements exist which can satisfy a requirement of $\mathcal{C}^1$-continuity, e.g. Hermitian finite elements and mixed finite elements [4, 6, 7, 8]. Unfortunately, these formulations are often not so robust, and can be limited to uniform and regular meshes. However, the requirement of higher-order continuity poses no issues when considering discretisation methods that can exploit rational basis functions, such as meshless methods [9], or isogeometric analysis.

Isogeometric analysis [10] can be conceived as a finite element framework where B-splines (or NURBS) are being used as the basis functions rather than the traditional Lagrange polynomials. B-splines, or nowadays rather their generalisation – Non-Uniform Rational B-Splines (NURBS) – have been widely used in Computer-Aided Geometric Design. Isogeometric analysis seeks to integrate the design and analysis processes by using the NURBS shape functions directly in analysis. For simple (one-patch) geometries, $\mathcal{C}^{p-1}$ continuity is achieved for NURBS of order p. The straightforward manner to achieve higher-order continuity with spline-based shape functions, has propelled their application in areas where higher-order continuity is necessary, such as gradient elasticity [11, 12, 13, 14, 15], gradient damage models [16], fluid flow in cracks of porous media [17], Kirchoff-Love shell theory [18, 19] and the Cahn-Hilliard equation [20, 21, 22], or when the properties of NURBS can be exploited to better capture localised deformation patterns such as shear bands [23].

Herein, we show how a plasticity theory with a gradient-dependent yield function is formulated and implemented exploiting isogeometric analysis. We employ Bézier extraction [24], which furnishes a convenient finite element data structure for analysis. The paper is organised as follows. Section 2 presents the incremental formulation of the governing equations for gradient plasticity, their weak forms, and succinctly discusses issues like the stress update algorithm and consistent tangent operator. In section 3, the governing equations are discretised in an isogeometric analysis framework, including the formulation of Bézier elements for NURBS and the unequal order interpolation for displacements and the plastic multiplier. Representative numerical examples are given in one and two dimensions, and some concluding remarks are drawn.

2. GRADIENT-DEPENDENT PLASTICITY

2.1. Incremental boundary value problem

Under static loading conditions and ignoring the effect of body forces, the equilibrium equation (in Voigt matrix notation) becomes:

$$\mathbf{L}^T \boldsymbol{\sigma} = \mathbf{0} \tag{1}$$

DOI: 10.1002/nme

where $\boldsymbol{\sigma} = (\sigma_{xx}, \sigma_{yy}, \sigma_{zz}, \sigma_{xy}, \sigma_{yz}, \sigma_{zx})^T$ is the stress tensor in vector form, and $\mathbf{L}$ is the differential operator:

$$\mathbf{L} = \begin{bmatrix} \frac{\partial}{\partial x} & 0 & 0 & \frac{\partial}{\partial y} & \frac{\partial}{\partial z} & 0 \\ 0 & \frac{\partial}{\partial y} & 0 & \frac{\partial}{\partial x} & 0 & \frac{\partial}{\partial z} \\ 0 & 0 & \frac{\partial}{\partial z} & 0 & \frac{\partial}{\partial x} & \frac{\partial}{\partial y} \end{bmatrix}^T . \tag{2}$$

Under the assumption of small displacement gradients, the following kinematic relation holds:

$$\boldsymbol{\varepsilon} = \mathbf{L}\mathbf{u} \tag{3}$$

with the strain vector $\boldsymbol{\varepsilon} = (\varepsilon_{xx}, \varepsilon_{yy}, \varepsilon_{zz}, \tau_{xy}, \tau_{yz}, \tau_{zx})^T$ and the displacement vector $\mathbf{u} = (u_x, u_y, u_z)^T$. The incremental constitutive relation between the stress and strain increments is expressed as:

$$\mathrm{d}\boldsymbol{\sigma} = \mathbf{D}^e(\,\mathrm{d}\boldsymbol{\varepsilon} - \mathrm{d}\boldsymbol{\varepsilon}^p) \tag{4}$$

where $\mathbf{D}^e$ is the elastic stiffness matrix and $\mathrm{d}\boldsymbol{\varepsilon}^p$ is the plastic strain increment vector. We adopt an associated plasticity flow rule,

$$\mathrm{d}\boldsymbol{\varepsilon}^p = \mathrm{d}\lambda\mathbf{m}, \quad \mathbf{m} = \frac{\partial F}{\partial \boldsymbol{\sigma}} \tag{5}$$

in which $\mathrm{d}\lambda$ is a non-negative plastic multiplier and $\mathbf{m}$ is a vector that defines the direction of plastic flow relative to the yield function F.

In the form of gradient plasticity which we consider, the yield function is made dependent not only on the invariant plastic strain measure (effective plastic strain), κ, but also on its Laplacian, $\nabla^2\kappa$:

$$F = F(\boldsymbol{\sigma}, \kappa, \nabla^2\kappa) \tag{6}$$

For isotropic hardening or softening, the gradient dependent yield function reduces to:

$$F = \Phi(\boldsymbol{\sigma}) - \bar{\boldsymbol{\sigma}}(\kappa, \nabla^2\kappa) \tag{7}$$

To relate the hardening parameter, κ, to the plastic multiplier, λ, the strain-hardening hypothesis is adopted in the remainder:

$$\mathrm{d}\kappa = \sqrt{\frac{2}{3}(\mathrm{d}\boldsymbol{\varepsilon}^p)^T\mathbf{Q}\mathrm{d}\boldsymbol{\varepsilon}^p} \tag{8}$$

in which $\mathbf{Q} = \mathrm{diag}[1, 1, 1, \frac{1}{2}, \frac{1}{2}, \frac{1}{2}]$.

Equations (1), (3) and (4) are complemented by the Karush-Kuhn-Tucker loading-unloading conditions:

$$\mathrm{d}\lambda \geq 0, \quad F \leq 0, \quad F\mathrm{d}\lambda = 0 \tag{9}$$

Finally, standard static and kinematic boundary conditions must be specified on complementary parts of the body surface S:

$$\boldsymbol{\Upsilon}\mathbf{n}_s = \mathbf{t}, \quad \mathbf{u} = \mathbf{u}_s \tag{10}$$

where $\boldsymbol{\Upsilon}$ denotes the stress tensor in matrix form, $\mathbf{n}_s$ is the outward normal to the surface S, and $\mathbf{t}$ is the boundary traction vector.

2.2. Weak formulation

Due to the gradient dependence of the yield function, second-order spatial derivatives of the hardening parameter, κ, need to be computed. For this purpose, the yield function, will be satisfied in a weak sense, at the end of every loading step. Consequently, the plastic strain field has to be discretised in addition to the discretisation of the displacements. This leads to the following coupled equations at iteration $j + 1$ of the current loading step:

$$\mathbf{L}^T\boldsymbol{\sigma}_{j+1} = \mathbf{0} \tag{11}$$

DOI: 10.1002/nme

$$F(\boldsymbol{\sigma}_{j+1}, \kappa_{j+1}, \nabla^2\kappa_{j+1}) = 0 \tag{12}$$

The weak form of these equations is obtained by setting:

$$\int_V \delta\mathbf{u}^T(\mathbf{L}^T\boldsymbol{\sigma}_{j+1})\mathrm{d}V = \mathbf{0} \tag{13}$$

and

$$\int_V \delta\lambda F(\boldsymbol{\sigma}_{j+1}, \kappa_{j+1}, \nabla^2\kappa_{j+1})\mathrm{d}V = 0 \tag{14}$$

where δ denotes the variation of a quantity. When Equation (13) is integrated by parts and the divergence theorem is invoked, the following equation ensues:

$$\int_V \delta\boldsymbol{\varepsilon}^T\boldsymbol{\sigma}_{j+1}\mathrm{d}V - \int_S \delta\mathbf{u}^T\mathbf{t}_{j+1}\mathrm{d}S = \mathbf{0} \tag{15}$$

We next decompose the stress at iteration $j+1$ as sum of the stress at the previous iteration and an increment: $\boldsymbol{\sigma}_{j+1} = \boldsymbol{\sigma}_j + \mathrm{d}\boldsymbol{\sigma}$. With Equations (4) and $(5)_1$, we obtain:

$$\int_V \delta\boldsymbol{\varepsilon}^T\mathbf{D}^e(\,\mathrm{d}\boldsymbol{\varepsilon} - \mathrm{d}\lambda\mathbf{m})dV = \int_S \delta\mathbf{u}^T\mathbf{t}_{j+1}\mathrm{d}S - \int_V \delta\boldsymbol{\varepsilon}^T\boldsymbol{\sigma}_j\mathrm{d}V \tag{16}$$

Through a Taylor's series expansion around $(\boldsymbol{\sigma}_j, \kappa_j, \nabla^2\kappa_j)$ and truncating after the linear terms, the yield function F can be developed as follows:

$$\begin{aligned} F(\boldsymbol{\sigma}_{j+1}, \kappa_{j+1}, \nabla^2\kappa_{j+1}) = F(\boldsymbol{\sigma}_j, \kappa_j, \nabla^2\kappa_j) + \left(\frac{\partial F}{\partial\boldsymbol{\sigma}}\right)^T\Bigg|_j \mathrm{d}\boldsymbol{\sigma} \\ + \frac{\partial F}{\partial\kappa}\Bigg|_j \mathrm{d}\kappa + \frac{\partial F}{\partial\nabla^2\kappa}\Bigg|_j \nabla^2(\mathrm{d}\kappa) \end{aligned} \tag{17}$$

where $\mathrm{d}\kappa = \kappa_{j+1} - \kappa_j$. Next, we define the hardening modulus, H:

$$H(\kappa, \nabla^2\kappa) = -\frac{\mathrm{d}\kappa}{\mathrm{d}\lambda}\frac{\partial F}{\partial\kappa} \tag{18}$$

and the gradient influence variable g:

$$g(\kappa) = \frac{\mathrm{d}\kappa}{\mathrm{d}\lambda}\frac{\partial F}{\partial\nabla^2\kappa} \tag{19}$$

and substitute them along with Equation $(5)_2$ into Equation (17) to obtain:

$$F(\boldsymbol{\sigma}_{j+1}, \kappa_{j+1}, \nabla^2\kappa_{j+1}) = F(\boldsymbol{\sigma}_j, \kappa_j, \nabla^2\kappa_j) + \mathbf{m}^T\mathrm{d}\boldsymbol{\sigma} - H\mathrm{d}\lambda + g\nabla^2(\mathrm{d}\lambda) \tag{20}$$

From a dimensional analysis, the gradient influence g must be proportional to a stiffness times a length squared. This (internal) length scale ℓ is an essential parameter of the gradient plasticity model, and in fact, of any gradient continuum model. It allows to model size effects [25] and also to obtain mesh-independent results for strain-softening continuum models.

Using Equations (4), (5) and (20), Equation (14) is now expressed as:

$$\begin{aligned} \int_{V_\lambda} \delta\lambda\big[\mathbf{m}^T\mathbf{D}^e\mathrm{d}\boldsymbol{\varepsilon} - (H + \mathbf{m}^T\mathbf{D}^e\mathbf{m})\mathrm{d}\lambda + g\nabla^2(\mathrm{d}\lambda)\big]dV = \\ - \int_{V_\lambda} \delta\lambda F(\boldsymbol{\sigma}_j, \kappa_j, \nabla^2\kappa_j)\mathrm{d}V \end{aligned} \tag{21}$$

where V_λ is the volume of the plastic region of the body. The values of $\mathbf{m}$, H and g are determined for the state defined by $(\boldsymbol{\sigma}_j, \kappa_j, \nabla^2\kappa_j)$. Integrating the Laplacian term in Equation (21) by parts, we

DOI: 10.1002/nme

obtain:

$$\int_{V_\lambda} \delta\lambda\big[\mathbf{m}^T\mathbf{D}^e\mathrm{d}\boldsymbol{\varepsilon} - (H + \mathbf{m}^T\mathbf{D}^e\mathbf{m})\mathrm{d}\lambda\big]dV - \int_{V_\lambda} g(\nabla\delta\lambda)^T(\nabla\mathrm{d}\lambda)\mathrm{d}V = \\ - \int_{V_\lambda} \delta\lambda F(\boldsymbol{\sigma}_j, \kappa_j, \nabla^2\kappa_j)\mathrm{d}V \tag{22}$$

and the following (non-standard) boundary conditions need to be fulfilled on S_λ, the boundary of the plastified part of the domain:

$$\delta\lambda = 0 \quad \text{or} \quad (\nabla\mathrm{d}\lambda)^T\mathbf{n}_\lambda = 0 \tag{23}$$

in which $\mathbf{n}_\lambda$ is the outward normal to the plastic region of the surface.

For finite increments, the elastic-plastic boundary moves stepwise as the plastic zone evolves. When this occurs, the first boundary condition Equation $(23)_1$ may not be satisfied and Equation $(23)_2$ must hold. This can be achieved either by enforcing Equation $(23)_2$ explicitly at S_λ, or by using $\mathcal{C}^1$-continuous basis functions for λ, so that the fact that $\lambda = 0$ on the entire elastic part of the domain directly leads to Equation $(23)_2$ to be satisfied at S_λ. It is noted that, different from Hermitian or mixed finite elements, where the derivatives of λ are required as independent degrees of freedom, the isogeometric formulation only requires the interpolation of λ, and no additional boundary conditions are necessary other than Equations (23).

2.3. Stress-strain relation and algorithmic tangent operator

The stress update in gradient plasticity follows the procedure from standard elastoplasticity. It is computed as an integral along a given path from the initial state $(\boldsymbol{\sigma}_0, \boldsymbol{\varepsilon}_0)$ to the final state $(\boldsymbol{\sigma}_j, \boldsymbol{\varepsilon}_j)$:

$$\boldsymbol{\sigma} = \boldsymbol{\sigma}_0 + \int_{\boldsymbol{\varepsilon}_0}^{\boldsymbol{\varepsilon}_j} \mathbf{D}^e\mathrm{d}\boldsymbol{\varepsilon} \tag{24}$$

The algorithmic stress update in iteration j follows the format [4]:

$$\boldsymbol{\sigma}_j = \boldsymbol{\sigma}_0 + \mathbf{S}(\boldsymbol{\varepsilon}_0, \boldsymbol{\Delta\varepsilon}_j) \tag{25}$$

where $\mathbf{S}$ is a non-linear mapping operator and $\boldsymbol{\Delta}$ is a total increment, i.e. sum of increments in all iterations for the current load step:

$$\boldsymbol{\Delta\varepsilon}_j = \sum_{i=1}^{j} \mathrm{d}\boldsymbol{\varepsilon}_i \tag{26}$$

The stress update in gradient plasticity uses an Euler backward algorithm [4]:

$$\boldsymbol{\sigma}_j = \boldsymbol{\sigma}_0 + \mathbf{D}^e\boldsymbol{\Delta\varepsilon}_j - \Delta\lambda_j\mathbf{D}^e\mathbf{m}_j. \tag{27}$$

The algorithmic or consistent tangent operator is defined as [4]:

$$\mathbf{D}^{alg} = \left.\frac{\partial\boldsymbol{\sigma}_j}{\partial\boldsymbol{\Delta\varepsilon}}\right|_{\boldsymbol{\varepsilon}_0, \boldsymbol{\Delta\varepsilon}_j} = \left.\frac{\partial\mathbf{S}}{\partial\boldsymbol{\Delta\varepsilon}}\right|_{\boldsymbol{\varepsilon}_0, \boldsymbol{\Delta\varepsilon}_j} \tag{28}$$

and is generally non-symmetric [26]. The full algorithm is summarised in Appendix A.

3. ISOGEOMETRIC DISCRETISATION

Herein, we use NURBS as shape functions and through Bézier extraction, cast them in an element data structure as in standard finite element analysis.

DOI: 10.1002/nme

3.1. NURBS shape functions

The basis functions of a univariate NURBS are given by:

$$R_{a,p}(\xi) = \frac{w_a B_{a,p}(\xi)}{\mathbf{W}(\xi)} \tag{29}$$

where $B_{a,p}$ is the basis function of the underlying B-spline, w_a is the corresponding NURBS weight and $\mathbf{W}$ is the weight function:

$$\mathbf{W}(\xi) = \sum_{b=1}^{n} w_b B_{b,p}(\xi) \tag{30}$$

The B-spline basis is defined for a polynomial of degree $p = 0$, as:

$$B_{a,0}(\xi) = \begin{cases} 1, & \xi_a \leq \xi \leq \xi_{a+1} \\ 0, & \text{otherwise} \end{cases} \tag{31}$$

and by the Cox-de Boor recursion formula for $p > 0$:

$$B_{a,p}(\xi) = \frac{\xi - \xi_a}{\xi_{a+p} - \xi_a} B_{a,p-1}(\xi) + \frac{\xi_{a+p+1} - \xi}{\xi_{a+p+1} - \xi_{a+1}} B_{a+1,p-1}(\xi) \tag{32}$$

where ξ is the parametric coordinate (knot) of a knot vector with increasing knot values:

$$\boldsymbol{\Xi} = \{\xi_1, \xi_2, \ldots, \xi_{n+p+1}\} \tag{33}$$

in which p is the polynomial degree and n is the number of basis functions. Projective transformations of B-splines in $\mathbb{R}^{d+1}$ produce NURBS in $\mathbb{R}^d$. Through a tensor product of the univariate NURBS bases, we obtain the two-dimensional NURBS shape functions:

$$N_{a,b}^{p,q}(\xi, \eta) = \frac{B_{a,p}(\xi) A_{b,q}(\eta) w_{a,b}}{\sum_{c=1}^{nB} \sum_{d=1}^{nA} B_{c,p}(\xi) A_{d,q}(\eta) w_{c,d}} \tag{34}$$

where η, $A_{b,q}$, q and nA are the knot vector, the B-spline basis, the polynomial degree and the number of basis functions in the second spatial dimension respectively. NURBS shape functions of order p are $\mathcal{C}^{p-1}$-continuous provided there are no repeated knots [10].

3.2. Bézier element

Different from Lagrange polynomials, NURBS basis functions are not local to an element. To facilitate isogeometric analysis in a classical finite element structure, the concept of Bézier extraction has been proposed [24]. In this approach, a NURBS mesh can be decomposed into $\mathcal{C}^0$-continuous Bézier elements through a Bézier extraction operator $\mathbf{C}$. While this gives a convenient element structure, it does not restrict the continuity of NURBS. For a two-dimensional element e, the NURBS shape functions become:

$$\mathbf{N}^e(\xi, \eta) = \mathbf{W}^e \mathbf{C}^e \frac{\mathbf{B}^e(\xi, \eta)}{W^e(\xi, \eta)} \tag{35}$$

with

$$W^e(\xi, \eta) = (\mathbf{w}^e)^T \mathbf{C}^e \mathbf{B}^e(\xi, \eta) \tag{36}$$

where $\mathbf{N}$ contains the NURBS basis functions, $\mathbf{w}$ is a vector of the NURBS weights, and $\mathbf{B}$ contains the Bézier basis functions (Bernstein polynomials). The procedure for computing the Bézier extraction operator of a NURBS has been presented in [24].

DOI: 10.1002/nme

3.3. Orders of interpolation

The displacement field, $\mathbf{u}$, and the plastic multiplier, λ, are discretised as follows:

$$\mathbf{u} = \mathbf{N}\mathbf{a} \tag{37}$$

$$\lambda = \mathbf{h}^T\mathbf{\Lambda} \tag{38}$$

where $\mathbf{a}$ is a vector of discrete displacements at the control points, $\mathbf{\Lambda}$ is a vector of the plastic multiplier degrees of freedom at the control point, $\mathbf{N}$ is a matrix, and $\mathbf{h}$, a vector, both containing NURBS shape functions. According to the linear kinematic relation in Equation (3), the strain vector can be expressed as:

$$\boldsymbol{\varepsilon} = \mathbf{B}\mathbf{a} \tag{39}$$

where $\mathbf{B} = \mathbf{L}\mathbf{N}$. In a similar way, we discretise the gradient of the plastic multiplier $\nabla\lambda$ and its Laplacian as:

$$\nabla\lambda = \mathbf{Q}^T\mathbf{\Lambda} \tag{40}$$

$$\nabla^2\lambda = \mathbf{p}^T\mathbf{\Lambda} \tag{41}$$

where

$$\mathbf{Q} = [\nabla h_1, \nabla h_2, \ldots, \nabla h_{ns}]^T \tag{42}$$

$$\mathbf{p} = [\nabla^2 h_1, \nabla^2 h_2, \ldots, \nabla^2 h_{ns}]^T \tag{43}$$

and ns is the number of shape functions at each control point.

The strain vector is one order lower than the displacement, cf. Equation (3). Since the plastic multiplier is of the same order as the (plastic) strain, the interpolation functions of the displacements, contained in $\mathbf{N}$, should be taken to be one order higher than those used for the plastic multiplier ($\mathbf{h}$). To satisfy the $\mathcal{C}^1$-continuity requirement, the NURBS shape functions in $\mathbf{h}$, must be, at least, of order two. Therefore, the shape functions in $\mathbf{N}$ are taken to be of the order three.

In isogeometric analysis, Bézier projection is generally required to construct conforming meshes of different orders and matching element boundaries. The procedure for achieving this has been presented in [17]. Starting with p-refinement, which elevates a NURBS from order p to order p', the control points for the p' curve/surface are computed for each element e as follows:

$$\mathbf{P}^{e,p'} = (\mathbf{R}^{e,p'})^T(\mathbf{E}^{p,p'})^T(\mathbf{C}^{e,p})^T(\mathbf{P}^{e,p}) \tag{44}$$

where $\mathbf{P}^{e,p}$ contains the control points of the initial curve/surface of order p, $\mathbf{P}^{e,p'}$ contains the control points of the target curve/surface of order p', $\mathbf{C}^{e,p}$ contains the initial Bézier extraction operator, $\mathbf{R}^{e,p'}$ is the inverse of the target Bézier extraction operator, i.e. $\mathbf{R}^{e,p'} = (\mathbf{C}^{e,p'})^{-1}$, and $\mathbf{E}^{p,p'}$ is the elevation matrix from degree p to p'. For a univariate elevation from quadratic to cubic NURBS, the elevation matrix is given by [17]:

$$\mathbf{E}^{2,3}_{uni} = \begin{bmatrix} 1 & \frac{1}{3} & 0 & 0 \\ 0 & \frac{2}{3} & \frac{2}{3} & 0 \\ 0 & 0 & \frac{1}{3} & 1 \end{bmatrix}. \tag{45}$$

The corresponding bivariate elevation matrix is obtained as a tensor product of the univariate matrices [24, 17]:

$$\mathbf{E}^{2,3}_{bi} = \mathbf{E}^{2,3}_{uni} \otimes \mathbf{E}^{2,3}_{uni} \tag{46}$$

When considering a one-dimensional 100 mm bar with one element, the initial quadratic knot vector is $\mathbf{\Xi}_2 = \{0, 0, 0, 1, 1, 1\}$ with control points $\mathbf{P}^{1,2} = [0 \quad 0;\ 50 \quad 0;\ 100 \quad 0]$ and the target cubic knot vector is $\mathbf{\Xi}_3 = \{0, 0, 0, 0, 1, 1, 1, 1\}$. Equation (44) then specialises as:

$$\left(\begin{bmatrix} 1 & 0 & 0 & 0 \\ 0 & 1 & 0 & 0 \\ 0 & 0 & 1 & 0 \\ 0 & 0 & 0 & 1 \end{bmatrix}^{-1} \right)^T \begin{bmatrix} 1 & \frac{1}{3} & 0 & 0 \\ 0 & \frac{2}{3} & \frac{2}{3} & 0 \\ 0 & 0 & \frac{1}{3} & 1 \end{bmatrix}^T \begin{bmatrix} 1 & 0 & 0 \\ 0 & 1 & 0 \\ 0 & 0 & 1 \end{bmatrix}^T \begin{bmatrix} 0 & 0 \\ 50 & 0 \\ 100 & 0 \end{bmatrix} = \begin{bmatrix} 0 & 0 \\ 33.3333 & 0 \\ 66.6667 & 0 \\ 100.000 & 0 \end{bmatrix} \tag{47}$$

DOI: 10.1002/nme

3.4. Spatial discretisation

The weak forms, Equations (16) and (21), are discretised using the interpolations of Equations (37) – (41). Requiring that the result holds for all admissible $\delta\mathbf{a}$ and $\delta\mathbf{\Lambda}$, we obtain the following set of non-linear algebraic equations [4]:

$$\begin{bmatrix} \mathbf{K}_{aa} & \mathbf{K}_{a\lambda} \\ \mathbf{K}_{\lambda a} & \mathbf{K}_{\lambda\lambda} \end{bmatrix} \begin{bmatrix} \mathrm{d}\mathbf{a} \\ \mathrm{d}\mathbf{\Lambda} \end{bmatrix} = \begin{bmatrix} \mathbf{f}_e + \mathbf{f}_a \\ \mathbf{f}_\lambda \end{bmatrix} \tag{48}$$

with the elastic stiffness matrix

$$\mathbf{K}_{aa} = \int_V \mathbf{B}^T \mathbf{D}^e \mathbf{B} \mathrm{d}V, \tag{49}$$

the off-diagonal matrices

$$\mathbf{K}_{a\lambda} = -\int_V \mathbf{B}^T \mathbf{D}^e \mathbf{m} \mathbf{h}^T \mathrm{d}V, \quad \mathbf{K}_{\lambda a} = \mathbf{K}_{a\lambda}^T, \tag{50}$$

the non-symmetric gradient-dependent matrix

$$\mathbf{K}_{\lambda\lambda} = \int_V [(H + \mathbf{m}^T \mathbf{D}^e \mathbf{m}) \mathbf{h}\mathbf{h}^T - g \mathbf{h}\mathbf{p}^T] \mathrm{d}V, \tag{51}$$

the external force vector

$$\mathbf{f}_e = \int_S \mathbf{N}^T \mathbf{t}_{j+1} \mathrm{d}S, \tag{52}$$

the vector of control point forces (equivalent to internal stresses)

$$\mathbf{f}_a = -\int_V \mathbf{B}^T \boldsymbol{\sigma}_j \mathrm{d}V, \tag{53}$$

and the vector of residual forces due to inexact fulfilment of the yield function

$$\mathbf{f}_\lambda = \int_V F(\boldsymbol{\sigma}_j, \lambda_j, \nabla^2 \lambda_j) \mathbf{h} \, \mathrm{d}V. \tag{54}$$

For associated flow, the gradient-dependent matrix can be made symmetric when Equation (22) is discretised instead of Equation (21):

$$\mathbf{K}_{\lambda\lambda} = \int_V [(H + \mathbf{m}^T \mathbf{D}^e \mathbf{m}) \mathbf{h}\mathbf{h}^T + g \mathbf{Q}\mathbf{Q}^T] \mathrm{d}V \tag{55}$$

It has been proposed to initially set the hardening modulus H equal to the Young's modulus E for elastic elements [4] in order to avoid singularity of the tangent operator for these elements. Also, when all elements are elastic, the gradient vector $\mathbf{m}$ is set to zero, and subsequently, $\mathbf{K}_{a\lambda} = \mathbf{K}_{a\lambda}^T = \mathbf{0}$.

4. NUMERICAL EXAMPLES

We demonstrate the suitability of isogeometric finite element analysis for gradient plasticity. In all examples considered, NURBS shape functions of order $p = 3$ have been used to discretise the displacements and for the plastic multiplier NURBS basis functions of order $p = 2$ have been employed. The non-symmetric formulation has been used.

DOI: 10.1002/nme

4.1. Gradient-dependent yield function

The Maxwell-Huber-Hencky-von Mises yield criterion is adopted for all numerical simulations:

$$F = \sqrt{\left(\frac{3}{2}\boldsymbol{\sigma}^T \mathbf{P} \boldsymbol{\sigma}\right)} - \bar{\boldsymbol{\sigma}}(\kappa, \nabla^2 \kappa) \tag{56}$$

where $\bar{\boldsymbol{\sigma}}_g$ is the gradient dependent yield strength and $\mathbf{P}$ is the symmetric projection matrix:

$$\mathbf{P} = \begin{bmatrix} \frac{2}{3} & -\frac{1}{3} & -\frac{1}{3} & 0 & 0 & 0 \\ -\frac{1}{3} & \frac{2}{3} & -\frac{1}{3} & 0 & 0 & 0 \\ -\frac{1}{3} & -\frac{1}{3} & \frac{2}{3} & 0 & 0 & 0 \\ 0 & 0 & 0 & 2 & 0 & 0 \\ 0 & 0 & 0 & 0 & 2 & 0 \\ 0 & 0 & 0 & 0 & 0 & 2 \end{bmatrix}. \tag{57}$$

The simple case of linear softening and a constant gradient influence variable (g) is considered. This renders the following form for the gradient-dependent yield strength:

$$\bar{\boldsymbol{\sigma}}(\kappa, \nabla^2 \kappa) = \sigma_y + H\kappa - g\nabla^2 \kappa, \quad g = -\ell^2 H \tag{58}$$

where σ_y is the initial yield strength and ℓ is the internal length scale introduced after Equation (20).

4.2. One-dimensional tensile bar with and without imperfection

A one-dimensional bar with specifications as listed in Table I and shown in Figure 1 is investigated using classical plasticity ($g = 0$) and gradient plasticity ($g = 50000$ N), cf. [4]. First, an ideally plastic homogeneous bar is considered, and then, in order to trigger localisation, a small imperfection is introduced in the central part of the bar. The stress and displacement at the right end are σ_r and $\bar{u}$ respectively. We consider two refined meshes with 2^6 and 2^7 elements respectively. For each mesh, four Gauss integration points are employed.

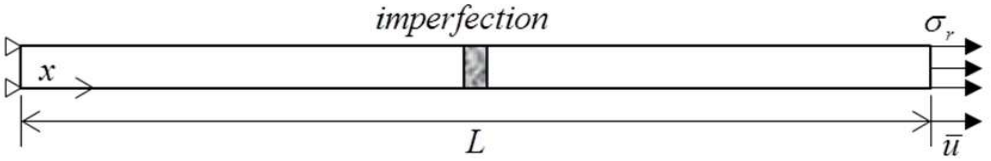

Figure 1. Tensile bar with imperfection

Specification	Notation	Value
Length	L	100 mm
Young's modulus	E	20000 N/mm^2
Tensile strength	σ_y	2 N/mm^2
Reduced tensile strength	σ_{yr}	1.8 N/mm^2
Softening modulus	H	-2000 N/mm^2
Gradient constant	g	50000 N
Thickness	t	1 mm

Table I. Specifications for one-dimensional tensile bar

Figure 2 shows the load-displacement diagram for a homogeneous bar assuming ideal plasticity ($H = 0$). A mesh of 64 elements is used. When $g = 0$, the result is identical with the classical plasticity algorithm. This remains the case even for $g = 50000$ N (corresponding to a length scale,

DOI: 10.1002/nme

$\ell = 5$ mm) indicating that there is no gradient influence. To trigger localisation, an imperfect zone is introduced at the middle of the bar. This is done by reducing the yield strength in the affected zone by 10%. The imperfection zone length is not very crucial [9], thus we use a length of 3.125 mm (two mid-elements).

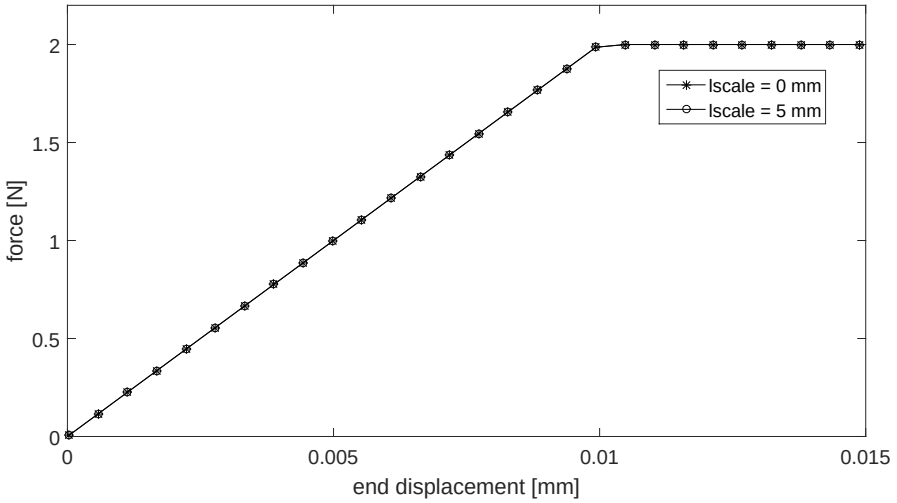

Figure 2. Perfectly plastic homogeneous bar without imperfection. 'lscale' represents length scale.

Results for the imperfect bar are shown in Figures 3 and 4. It is evident from the load-displacement diagram that there is no mesh dependence. In fact, the slope of the softening regime matches the analytical solution perfectly, cf. [2]. The cosine distribution of the effective plastic strain that comes from the analytical solution is also reproduced. A localisation zone width of $10\pi \approx 31.4$ mm was calculated analytically. This closely matches the localisation zone widths for both discretisations, see Figure 4. It is noted that for $\ell = 5$ mm, the load-displacement curve shows a sharp cusp beyond an end displacement of 0.02 mm [2]. This leads to non-symmetric evolution of the plastic strain distribution. Thus, to conveniently compare the results with the analytical solution, the maximum end displacement has been chosen before the cusp develops.

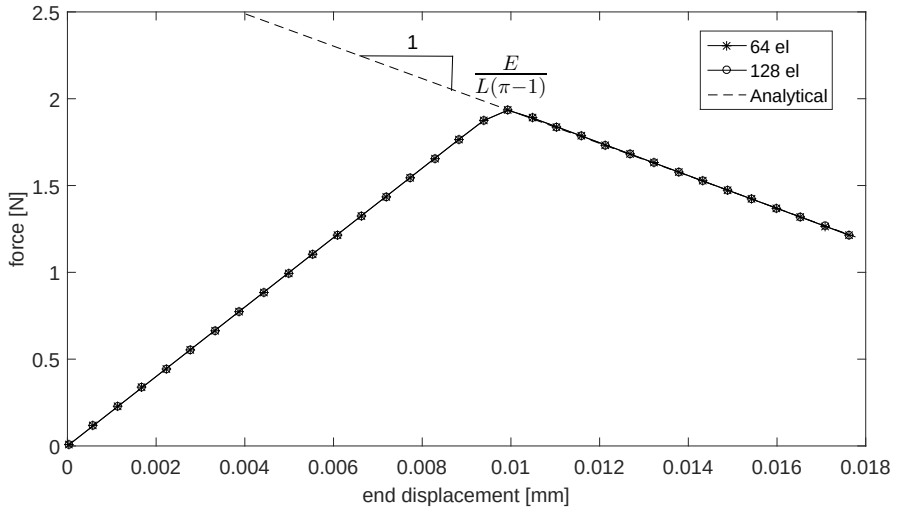

Figure 3. Imperfect bar: Load-displacement diagrams for discretisations with 64 and 128 elements (el).

DOI: 10.1002/nme

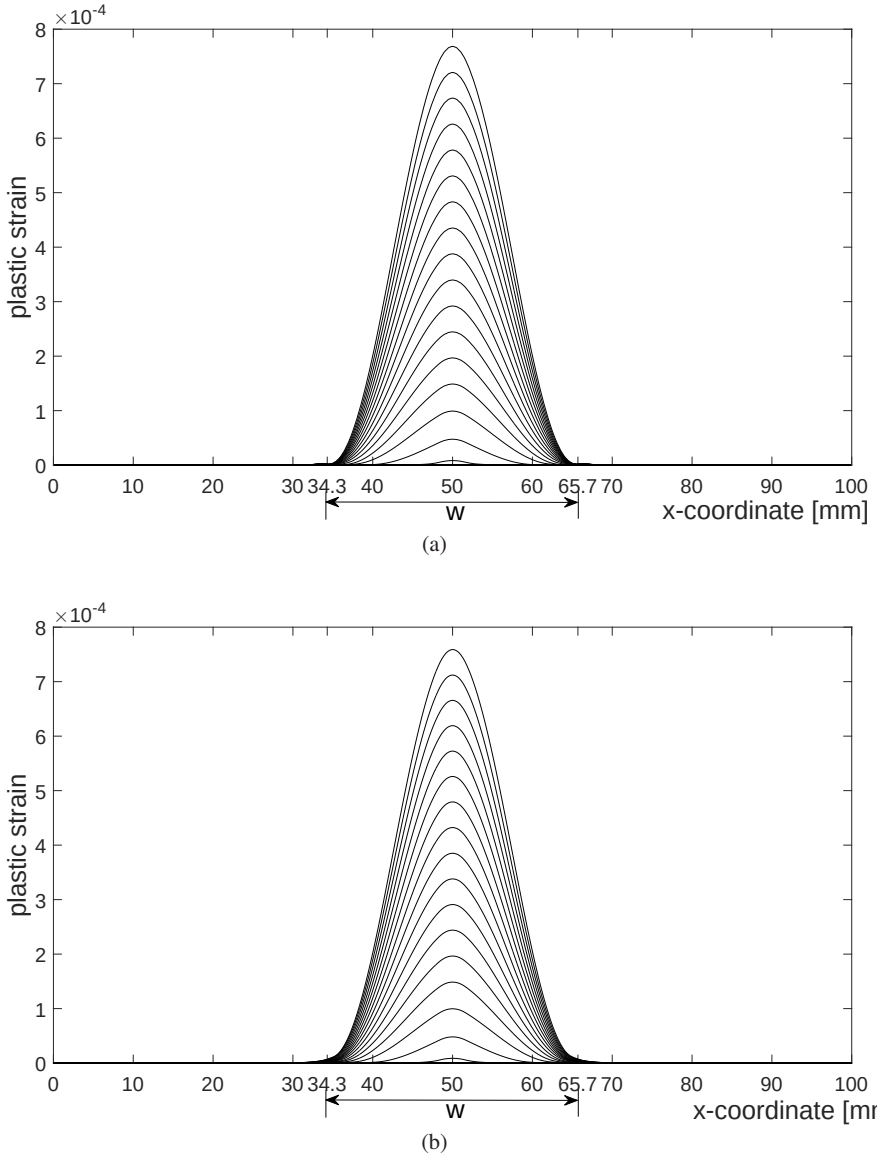

Figure 4. Evolution of effective plastic strain for the bar with imperfection discretised with (a) 64 elements and (b) 128 elements. w is the analytical solution: $10\pi \approx 31.4$ mm.

Figure 5 exhibits stress oscillations which do not disappear upon mesh refinement. This was also observed using the element-free Galerkin method [9] and is due to the satisfaction of the yield function in a weak sense rather than in a point-wise fashion. The norm of non-standard residuals does not fully converge to zero, and neither does the norm of out-of-balance forces.

4.3. Two-dimensional panel under uniaxial tension

Next, we consider a square panel subjected to uniaxial tension as shown in Figure 6 with material properties summarised in Table II, cf. [27, 28]. The left edge is restricted in the x-direction with its midpoint fixed in both directions, while the right edge is pulled in the x-direction. In order to avoid a homogeneous deformation with no gradient effect, some elements at the bottom-left corner have been weakened. We consider two meshes with $2^4 \times 2^4$ and $2^5 \times 2^5$ elements, respectively.

DOI: 10.1002/nme

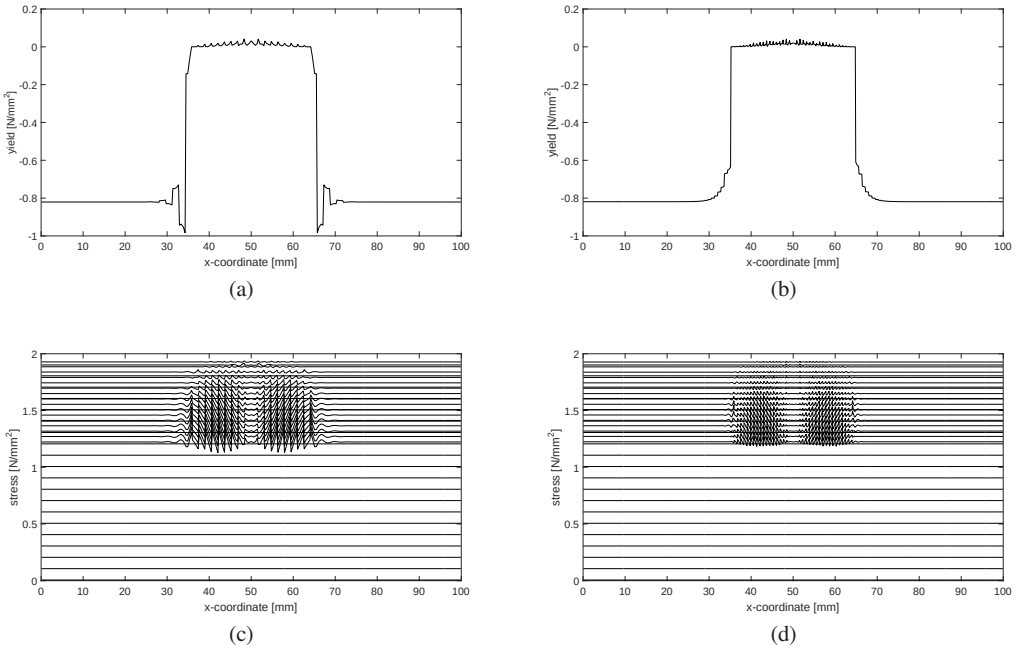

Figure 5. Non-zero values of the yield function in the final step – (a),(b), and evolution of stress oscillations – (c),(d) for the imperfect bar discretised with 64 elements (left) and 128 elements (right).

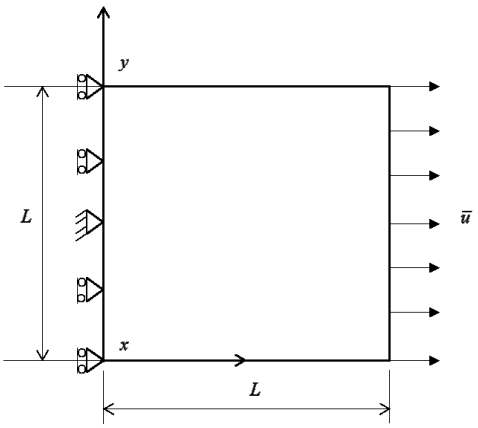

Figure 6. Geometry and boundary conditions of square panel under uniaxial tension.

Specification	**Notation**	**Value**
Length	L	10 mm
Young's modulus	E	20000 N/mm^2
Poisson ratio	ν	0.25
Tensile strength	σ_y	2 N/mm^2
Reduced tensile strength	σ_{yr}	1.8 N/mm^2
Softening modulus	H	-400 N/mm^2
Gradient constant	g	100 N ($\ell = 0.5$ mm)
		400 N ($\ell = 1.0$ mm)

Table II. Specifications for square panel under tension.

DOI: 10.1002/nme

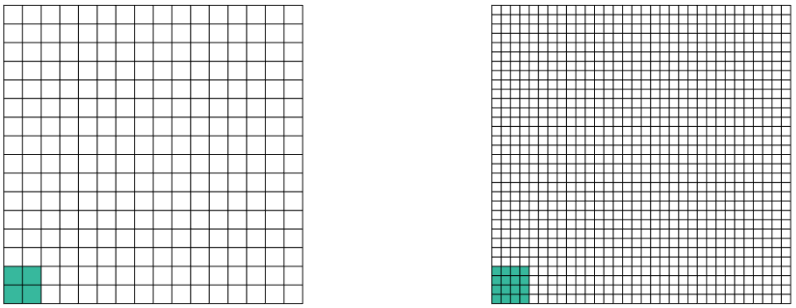

(a) (b)

Figure 7. Meshes of square panel showing weakened elements: (a) 256 elements; (b) 1024 elements.

The two meshes and the corresponding weak elements with a 10% reduction in yield strength are shown in Figure 7. Starting from the region of weak elements, a localisation band develops. This is depicted in Figure 8. For classical plasticity (Figure 8(a) and (b)), the localisation width is strongly mesh dependent. This also becomes clear from the load-displacement diagram of Figure 9(a), where the curve using 256 elements deviates from the discretisation with 1024 elements. It is noted that the difference is moderate due to the fact that in this example only a moderate rate of softening has been used ($H/E = -0.02$). A rather moderate rate of softening was chosen since otherwise convergence problems were encountered for this two-dimensional problem.

When an internal length scale is introduced, unsurprisingly, results are obtained that are fully mesh-objective. This is very clear from the contour plots for the effective plastic strain, Figures 8(c)-(d) for an internal length scale $\ell = 0.5$ mm, and Figures 8(e)-(f) for an internal length scale $\ell = 1.0$ mm. It is noted that for convenience, the scales of plots comparing classical and gradient plasticity have been synchronised. Comparing the contour plots for $\ell = 0.5$ mm on one hand, and those for $\ell = 1.0$ mm, on the other hand, we clearly observe that the width of the localisation zone is proportional to the internal length scale. Figures 9 also show full mesh-objectivity when a gradient dependence is introduced in the yield function, and confirm that for higher values of ℓ a more ductile behaviour is obtained, which is concomitant with an increased width of the localisation zone.

The finite element size needs to be smaller than the internal length scale for sufficient accuracy to be achieved [29]. This was observed for a coarser mesh (8×8 elements with a finite element size of 1.25 mm) where the load-displacement curve failed to converge for $\ell = 0.5$ mm. In transient finite element analysis which tries to accurately capture the propagation of plastic strain, the observation implies that the size of the finite elements should be small relative to the size of the structure. Adaptive remeshing may therefore be required particularly in the localisation area [3, 29].

As emphasised in [30], contour plots are important in assessing higher-order NURBS elements in plasticity as load-displacement diagrams may not be sufficient. The least squares approach [30, 31] has been used for plotting the effective plastic strain contours employing the relevant (quadratic) shape functions. A brief description of how to extrapolate the effective plastic strain values from Gauss points to control points is given in Appendix B.

DOI: 10.1002/nme

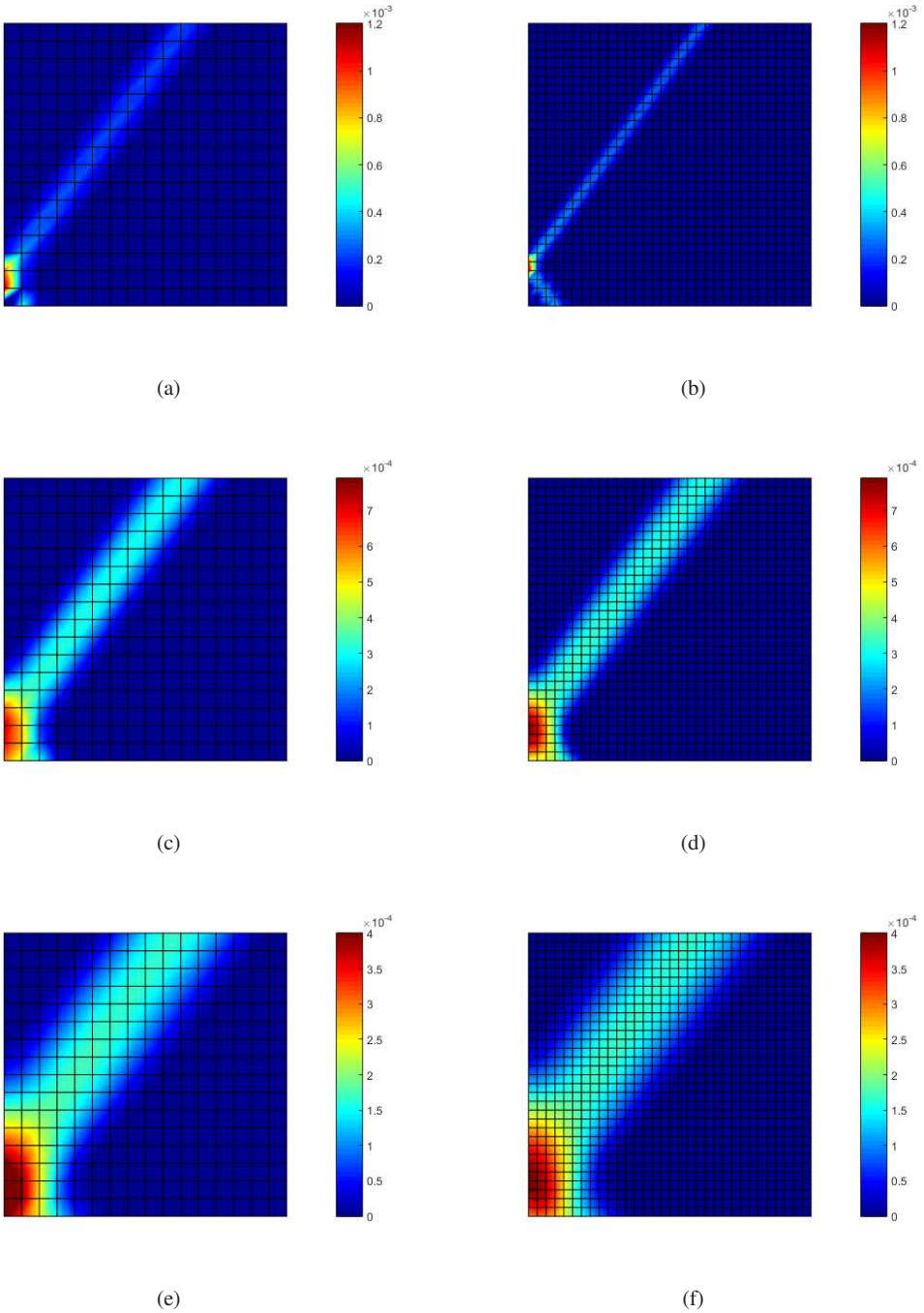

Figure 8. Square panel: Distribution of effective plastic strain measure (κ) for the case of classical plasticity – (a) and (b), and gradient plasticity for $\ell = 0.5$ mm – (c) and (d), as well as $\ell = 1.0$ mm – (e) and (f).

DOI: 10.1002/nme

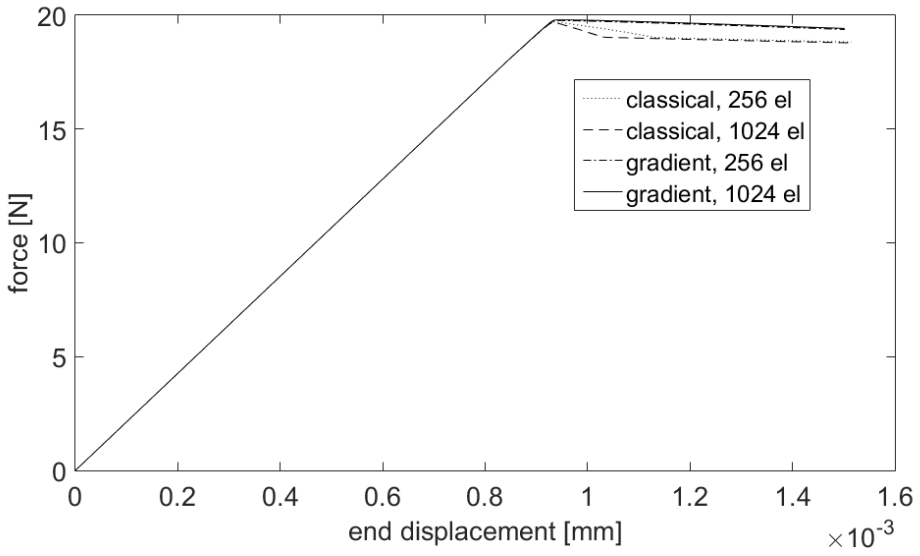

(a)

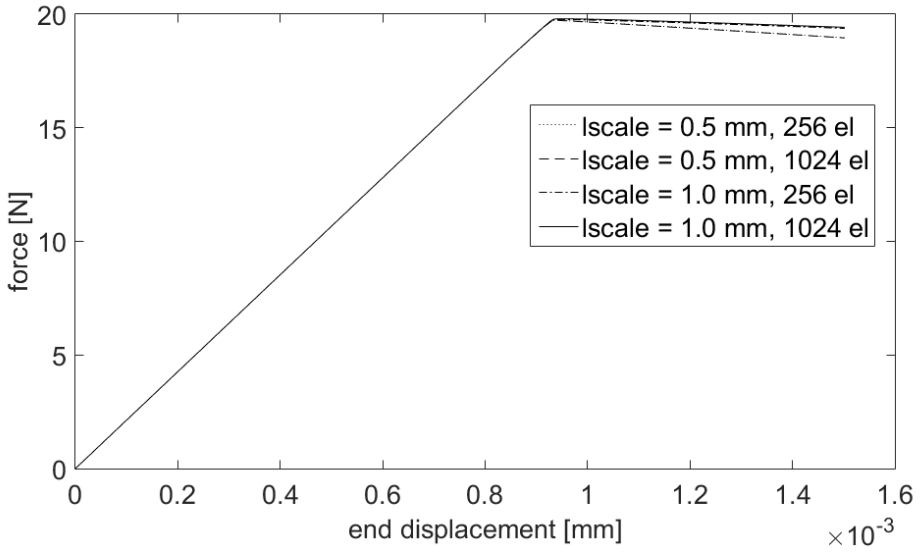

(b)

Figure 9. Load-displacement diagrams for square panel (a) using classical plasticity ($\ell = 0$ mm) and gradient plasticity with $\ell = 0.5$ mm and (b) using gradient plasticity with $\ell = 0.5$ mm and $\ell = 1.0$ mm.

DOI: 10.1002/nme

5. CONCLUDING REMARKS

An isogeometric approach to gradient-dependent plasticity has been presented. Compared to finite element or meshless approaches, isogeometric analysis has the advantage that the displacements and the plastic multiplier can be interpolated with different orders in a straightforward manner, which enables a consistent, equal-order approximation of the strains and the plastic strains. Herein, we have employed NURBS with a cubic interpolation for the displacements and a quadratic interpolation for the plastic multiplier. Through Bézier projection, meshes with matching element boundaries have been obtained.

Compared to finite element approaches that use Hermitian shape functions for the plastic multiplier or mixed finite element approaches, isogeometric analysis has the distinct disadvantage that no interpolation of derivatives is required. This advantage shows up especially in the boundary conditions, where no non-physical constraints have to be imposed.

The ability of gradient plasticity to maintain the well-posedness of the governing equations for softening problems with the ensuing band width that is mesh-independent, has been demonstrated in an isogeometric analysis framework for one-dimensional and two-dimensional boundary value problems.

APPENDIX A

Box 1. Algorithm for $\mathcal{C}^1$ formulation of gradient plasticity (iteration $j+1$)

1. Compute the matrices $\mathbf{K}_{aa}$, $\mathbf{K}_{a\lambda}$, $\mathbf{K}_{\lambda a}$ and $\mathbf{K}_{\lambda\lambda}$, and forces $\mathbf{f}_e$, $\mathbf{f}_a$ and $\mathbf{f}_\lambda$, according to Equations (49) – (54) while replacing $\mathbf{D}^e$ with $\mathbf{D}^{alg}$
2. Solve for $\mathrm{d}\mathbf{a}$ and $\mathrm{d}\boldsymbol{\Lambda}$ using Equation (48)
3. Update the total increments $\Delta\mathbf{a}_{j+1} = \Delta\mathbf{a}_j + \mathrm{d}\mathbf{a}$, and $\Delta\boldsymbol{\Lambda}_{j+1} = \Delta\boldsymbol{\Lambda}_j + \mathrm{d}\boldsymbol{\Lambda}$.
4. Compute the following at each integration point:
   $\Delta\boldsymbol{\varepsilon}_{j+1} = \mathbf{B}\Delta\mathbf{a}_{j+1}$,
   $\Delta\lambda_{j+1} = \mathbf{h}^T\Delta\boldsymbol{\Lambda}_{j+1}$,
   $\nabla^2(\Delta\lambda_{j+1}) = \mathbf{p}^T\Delta\boldsymbol{\Lambda}_{j+1}$,
   $\kappa_{j+1} = \kappa_0 + \Delta\lambda_{j+1}$,
   $\nabla^2\kappa_{j+1} = \nabla^2\kappa_0 + \nabla^2(\Delta\lambda_{j+1})$,
   trial stress $\boldsymbol{\sigma}_t = \boldsymbol{\sigma}_0 + \mathbf{D}^e\Delta\boldsymbol{\varepsilon}_{j+1}$.
   If $F(\boldsymbol{\sigma}_{j+1}, \kappa_{j+1}, \nabla^2\kappa_{j+1}) > 1\times10^{-6}$,
      then plastic state:
         compute $\mathbf{m}_t$
         $\boldsymbol{\sigma}_{j+1} = \boldsymbol{\sigma}_t - \Delta\lambda_{j+1}\mathbf{D}^e\mathbf{m}_t$
         compute the algorithmic stiffness operator
         compute H for the next iteration,
      else elastic state:
         $\mathbf{m}_t = \mathbf{0}$
         $\boldsymbol{\sigma}_{j+1} = \boldsymbol{\sigma}_t$
         $\mathbf{D}^{alg} = \mathbf{D}^e$
         $H = E$
5. Check the global convergence criterion. If not converged, go to 1.

$(\bullet)_0$ denotes value at previous converged load step and $(\bullet)_j$ indicates value at previous iteration.

APPENDIX B

History variables are normally computed at integration points. However, these variables must be extrapolated to the control points for post-processing purposes. Herein, we have adopted a global

DOI: 10.1002/nme

least-squares fit to extrapolate the effective plastic strain from the Gauss points to the control points. The control variables contained in the vector $\boldsymbol{\kappa}^c$ are obtained from the Gauss point values contained in the vector $\boldsymbol{\kappa}^g$ by solving [31]:

$$\mathbf{M}\boldsymbol{\kappa}^c = \int_V \mathbf{h}^T \boldsymbol{\kappa}^g \mathrm{d}V \tag{59}$$

where $\mathbf{M}$ is the least-squares fit matrix or Gramm matrix given by:

$$\mathbf{M} = \int_V \mathbf{h}\mathbf{h}^T \mathrm{d}V \tag{60}$$

and $\mathbf{h}$ a vector that contains the NURBS shape functions used for discretising the plastic multiplier as in Equation (38). The same approach can be used for other history variables.

REFERENCES

1. Bazant ZP, Belytschko TB, Chang TP. Continuum theory for strain-softening. *Journal of Engineering Mechanics* 1984; **110**:1666–1692.
2. de Borst R, Mühlhaus HB. Gradient-dependent plasticity: Formulation and algorithmic aspects. *International Journal for Numerical Methods in Engineering* 1992; **35**:521–539.
3. de Borst R, Sluys LJ, Muhlhaus HB, Pamin J. Fundamental issues in finite element analyses of localization of deformation. *Engineering Computations* 1993; **10**:99–121.
4. de Borst R, Pamin J. Some novel developments in finite element procedures for gradient-dependent plasticity. *International Journal for Numerical Methods in Engineering* 1996; **39**:2477–2505.
5. Mühlhaus HB, Alfantis EC. A variational principle for gradient plasticity. *International Journal of Solids and Structures* 1991; **28**:845–857.
6. Fredriksson P, Gudmundson P, Mikkelsen LP. Finite element implementation and numerical issues of strain gradient plasticity with application to metal matrix composites. *International Journal of Solids and Structures* 2009; **46**:3977–3987.
7. Mroginski JL, Etse G. A finite element formulation of gradient-based plasticity for porous media with C1 interpolation of internal variables. *Computers and Geotechnics* 2013; **49**:7–17.
8. Miehe C, Aldakheel F, Mauthe S. Mixed variational principles and robust finite element implementations of gradient plasticity at small strains. *International Journal for Numerical Methods in Engineering* 2013; **94**:1037–1074.
9. Pamin J, Askes H, de Borst R. Two gradient plasticity theories discretized with the element-free Galerkin method. *Computer Methods in Applied Mechanics and Engineering* 2003; **192**:2377–2403.
10. Hughes TJR, Cottrell JA, Bazilevs Y. Isogeometric analysis: CAD, finite elements, NURBS, exact geometry and mesh refinement. *Computer Methods in Applied Mechanics and Engineering* 2005; **194**:4135–4195.
11. Fischer P, Klassen M, Mergheim J, Steinmann P, Müller R. Isogeometric analysis of 2D gradient elasticity. *Computational Mechanics* 2011; **47**:325–334.
12. Malagù M, Benvenuti E, Duarte C, Simone A. One-dimensional nonlocal and gradient elasticity: Assessment of high order approximation schemes. *Computer Methods in Applied Mechanics and Engineering* 2014; **275**:138–158.
13. Rudraraju S, van der Ven A, Garikipati K. Three-dimensional isogeometric solutions to general boundary value problems of Toupin's gradient elasticity theory at finite strains. *Computer Methods in Applied Mechanics and Engineering* 2014; **278**:705–728.
14. Niiranen J, Khakalo S, Balobanov V, Niemi AH. Variational formulation and isogeometric analysis for fourth-order boundary value problems of gradient-elastic bar and plane strain/stress problems. *Computer Methods in Applied Mechanics and Engineering* 2016; **308**:182–211.
15. Lale E, Zhou X, Cusatis G. Isogeometric implementation of high-order microplane model for the simulation of high-order elasticity, softening, and localization. *Journal of Applied Mechanics* 2017; **84**:011 005.
16. Verhoosel CV, Scott MA, Hughes TJR, de Borst R. An isogeometric analysis approach to gradient damage models. *International Journal for Numerical Methods in Engineering* 2011; **86**:115–134.
17. Vignollet J, May S, de Borst R. Isogeometric analysis of fluid-saturated porous media including flow in the cracks. *International Journal for Numerical Methods in Engineering* 2016; **108**:990–1006.
18. Kiendl J, Bletzinger KU, Linhard J, Wüchner R. Isogeometric shell analysis with Kirchhoff–Love elements. *Computer Methods in Applied Mechanics and Engineering* 2009; **198**:3902–3914.
19. May S, Vignollet J, de Borst R. Powell-Sabin B-splines and unstructured standard T-splines for the solution of Kichhoff-Love plate theory using Bézier extraction. *International Journal for Numerical Methods in Engineering* 2016; **107**:205–233.
20. Gómez H, Calo VM, Bazilevs Y, Hughes TJR. Isogeometric analysis of the Cahn–Hilliard phase-field model. *Computer Methods in Applied Mechanics and Engineering* 2008; **197**:4333–4352.
21. Liu J, Dedè L, Evans JA, Borden MJ, Hughes TJR. Isogeometric analysis of the advective Cahn–Hilliard equation: Spinodal decomposition under shear flow. *Journal of Computational Physics* 2013; **242**:321–350.
22. Kästner M, Metsch P, de Borst R. Isogeometric analysis of the Cahn–Hilliard equation–a convergence study. *Journal of Computational Physics* 2016; **305**:360–371.
23. Berger-Vergiat L, McAuliffe C, Waisman H. Isogeometric analysis of shear bands. *Computational Mechanics* 2014; **28**:503–521.

DOI: 10.1002/nme

24. Borden MJ, Scott MA, Evans JA, Hughes TJR. Isogeometric finite element data structures based on Bézier extraction of NURBS. *International Journal for Numerical Methods in Engineering* 2011; **87**:15–47.
25. de Borst R, Gutiérrez MA. A unified framework for concrete damage and fracture models including size effects. *International Journal of Fracture* 1999; **95**:261–277.
26. Ortiz M, Martin JB. Symmetry-preserving return mapping algorithms and incrementally extremal paths: a unification of concepts. *International Journal for Numerical Methods in Engineering* 1989; **28**:1839–1854.
27. Liebe T, Menzel A, Steinmann P. Theory and numerics of geometrically non-linear gradient plasticity. *International Journal of Engineering Science* 2003; **41**:1603–1629.
28. Yang Y, Misra A. Higher-order stress-strain theory for damage modeling implemented in an element-free Galerkin formulation. *CMES-Computer Modeling in Engineering & Sciences* 2010; **64**:1–36.
29. Huerta A, Pijaudier-Cabot G. Discretization influence on regularization by two localization limiters. *Journal of Engineering Mechanics* 1994; **120**:1198–1218.
30. Elguedj T, Hughes TJR. Isogeometric analysis of nearly incompressible large strain plasticity. *Computer Methods in Applied Mechanics and Engineering* 2014; **268**:388–416.
31. Mitchell TJ, Govindjee S, Taylor RL. A method for enforcement of Dirichlet boundary conditions in isogeometric analysis. *Recent Developments and Innovative Applications in Computational Mechanics*. Springer, 2011; 283–293.

DOI: 10.1002/nme